Slow light in periodic superstructure Bragg gratings

D. Janner, G. Galzerano, G. Della Valle, P. Laporta, and S. Longhi
Dipartimento di Fisica and Istituto di Fotonica e Nanotecnologie del CNR, Politecnico di Milano, Piazza L. da Vinci 32, I-20133 Milano, Italy

M. Belmonte
Avanex Corporation, Via F. Fellini 4, I-20097 San Donato Milanese, Italy
(Received 28 June 2005; published 8 November 2005)

A theoretical and experimental analysis of group velocity reduction in periodic superstructure Bragg gratings is presented. Experimental demonstration of group velocity reduction of sub-nanosecond pulses at the 1.5 μm wavelength of optical communications is reported using a Moiré fiber grating.

DOI: 10.1103/PhysRevE.72.056605 PACS number(s): 42.70.Qs, 42.79.Dj, 42.81.Qb

I. INTRODUCTION

The possibility to control the group velocity of light by exploiting strong resonances in either atomic or photonic systems has received a tremendous interest in the past few years, with spectacular results of strong light slowing down and even light freezing obtained in coherent atom-photon interactions (for reviews on this subject see, for instance, [1–4] and references therein). The possibility of advancing or slowing light using simple solid-state-based technology compatible with conventional lightwave circuits, such as optical fibers [5–8], coupled-resonator optical waveguides and microrings [4,9,10], and photonic crystal waveguides [11,12], is currently viewed as a key issue of realizing fast-access memories and all-optical buffers for future optical communication networks. Fiber-based structures may offer the advantage of a full compatibility with current fiber-optic communication systems, though group index change and bandwidths may be modest as compared to, e.g., coupled-resonator microring or planar photonic crystal-based structures. Slow light in nonstructured optical fibers has been recently proposed and demonstrated using stimulated Brillouin scattering [7,8]. Though this technique allows for a broad tunability, the low group index enhancement and narrow bandwidth of Brillouin gain curves require long interaction lengths (a few hundreds of meters) and long pulses (few tens of nanoseconds at least). The use of structured fibers, such as fiber Bragg gratings, may provide stronger group index enhancements, compactness, and a wider bandwidth, at the expense of a narrow tunability. Powerful synthesis and writing techniques of fiber Bragg gratings have been already allowed to achieve complex and precise manipulation and coherent control of pulse propagation at the wavelength of optical communications (see, for instance, [13] and references therein). Moiré gratings, a special example of superstructure periodic Bragg gratings, have been recently proposed as potential slow wave structures with low dispersive effects [14], however, an experimental demonstration of group velocity reduction in such structures has not been reported yet. The basic physical principle underlying light slowing down with low dispersion in a dual-periodic Bragg grating, such as in the Moiré grating structures [14], is due to the opening of a narrow transmission band in the band gap of the periodic structure associated with strong light localization [15].

In this work we study superstructure Bragg gratings for slow light and report the experimental observation of group velocity reduction (by a factor up to $\simeq 2$) of subnanosecond pulses at the 1.5 μm wavelength of optical communications using home made Moiré fiber gratings. In Sec. II we provide general results on slow light in superstructure periodic Bragg gratings using a coupled-mode equation approach. In Sec. III an experimental demonstration of group velocity reduction is reported for subnanosecond pulses at a 1.5 μm wavelength in a 20-cm long Moiré fiber grating. Finally, in Sec. IV the main conclusions are outlined.

II. THEORETICAL ANALYSIS

The starting point of our analysis is provided by a standard coupled-mode equation analysis of wave propagation in periodic dielectric media with a shallow grating profile, which is well suited to study, e.g., light propagation in fiber Bragg gratings [16]. The grating profile, in the case of a periodic (i.e., not chirped) structure, has the form

$$n(z) = n_0 + \Delta n a(z) \cos(2k_B z), \tag{1}$$

where n_0 is the bulk refractive index, Δn is the maximum refractive index change of the grating, $2k_B$ is the spatial frequency of the rapidly varying periodic grating which determines the Bragg frequency $\omega_B = k_B c_0 / n_0$ around which the structure shows a band gap, and $a(z)$ is the normalized profile of the grating amplitude [$|a(z)| \leqslant 1$], which is assumed to vary slowly as compared to the grating period π / k_B. For a superstructure grating, which is of interest in this work, the amplitude profile $a(z)$ is periodic with a period $\Lambda_S \gg \pi / k_B$, i.e., $a(z + \Lambda_S) = a(z)$ [see Fig. 1(a)]. A monochromatic field $\mathcal{E}(z,t)$ at frequency ω close to the Bragg frequency ω_B propagating into the dielectric grating can be written as a superposition of forward and backward waves according to

$$\mathcal{E}(z,t) = u(z)\exp(-i\omega t + ik_B z) + v(z)\exp(-i\omega t - ik_B z) + \text{c.c.}, \tag{2}$$

where $u(z)$ and $v(z)$ are the amplitudes of forward and backward propagating waves which satisfy the coupled-mode equations [17]:

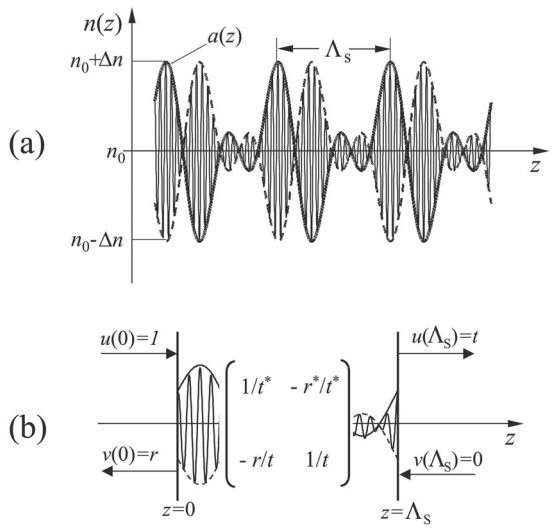

FIG. 1. (a) Schematic of the refractive index profile of a periodic superstructure Bragg grating. The bold solid line is the amplitude profile $a(z)$ of the superstructure. (b) Transfer matrix and transmission and/or reflection spectral coefficients for a single cell of the superstructure.

$$\frac{du}{dz} = i\delta u + iq(z)v, \tag{3}$$

$$\frac{dv}{dz} = -i\delta v - iq(z)u. \tag{4}$$

In Eqs. (3) and (4), $\delta = n_0(\omega - \omega_B)/c_0$ is the wave-number detuning parameter and $q(z) = [k_B \Delta n/(2n_0)]a(z)$ is the real-valued scattering potential. Note that $|u|^2 - |v|^2$ is an invariant for Eqs. (3) and (4) owing to energy conservation and, for a finite grating length, its value depends on boundary conditions at input and output grating planes. The total grating length L is assumed to be either infinite (whenever finite boundary effects are negligible) or an integer multiple of the superstructure period Λ_S, i.e., $L = N\Lambda_S$, where N is the number of cells. Owing to the periodicity of $a(z)$, the propagation properties of an infinite structure (as well as of a N-cell structure), including location of photonic band gaps and band dispersion curves, can be easily derived from the analysis of a single cell of the superstructure using standard techniques (see, for instance, [18]). In fact, let us indicate by $t = t(\omega)$ and $r = r(\omega)$ the transmission and reflection field coefficients of a single cell of the superstructure [see Fig. 1(b)], so that one can write:

$$\begin{pmatrix} u(\Lambda_S) \\ v(\Lambda_S) \end{pmatrix} = \begin{pmatrix} \frac{1}{t^*} & -\frac{r^*}{t^*} \\ -\frac{r}{t} & \frac{1}{t} \end{pmatrix} \begin{pmatrix} u(0) \\ v(0) \end{pmatrix}, \tag{5}$$

where $*$ denotes complex conjugate. If we consider an infinitely-long grating structure, a Floquet-Bloch solution to the periodic system [Eqs. (3) and (4)] has the form

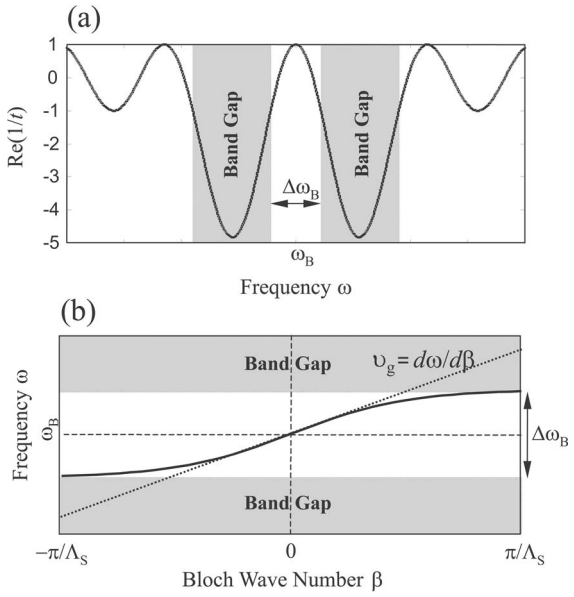

FIG. 2. (a) Typical behavior of $\mathrm{Re}(1/t)$ versus frequency ω in a periodic superstructure with a zero-mean value for $a(z)$. Note that a narrow transmission band of width $\Delta\omega_B$ is opened inside two band-gap regions. (b) Qualitative behavior of the dispersion curve $\omega = \omega(\beta)$ of the transmission band in a periodic superstructure [Eq. (7)]. The slope of the dotted line is the group velocity of a pulse tuned at $\omega = \omega_B$.

$$\begin{pmatrix} u(z) \\ v(z) \end{pmatrix} = \begin{pmatrix} \tilde{u}(z) \\ \tilde{v}(z) \end{pmatrix} \exp(i\beta z), \tag{6}$$

where $\tilde{u}(z)$ and $\tilde{v}(z)$ are periodic functions with period Λ_S, and β is the Bloch wave number, which is chosen in the first Brillouin zone $(-\pi/\Lambda_S < \beta \leq \pi/\Lambda_S)$. Note that β depends parametrically on the wave number detuning δ, i.e., on the frequency ω of the propagating wave. A comparison of Eqs. (5) and (6) shows that the following relation exists between the transmission field coefficient t of the single cell of the superstructure and the Bloch wave number β of the infinite superstructure

$$\cos(\beta\Lambda_S) = \mathrm{Re}\left(\frac{1}{t(\omega)}\right). \tag{7}$$

Note that Eq. (7) implicitly defines the dispersion curve $\beta = \beta(\omega)$ of Bloch waves once the transmission coefficient $t(\omega)$ of the single cell has been calculated by, e.g., a numerical analysis of Eqs. (3) and (4) in one period. In particular, a band gap (corresponding to an imaginary value of propagation constant β) occurs at frequencies where $|\mathrm{Re}(1/t)| > 1$. We recall that for a periodic uniform grating $[a(z) = 1]$, a band gap of width $\Delta\omega_{GAP} = \omega_B \Delta n/n_0$ occurs, which is centered at $\omega = \omega_B$. For a modulation amplitude $a(z)$ of the superstructure with zero-mean value $[\int_0^{\Lambda_S} a(z)dz = 0]$, which is the case of a major interest for light slowing down, a narrow transmission window centered at $\omega = \omega_B$ is opened inside the band gap, as shown in Fig. 2. In the figure is also shown a qualitative behavior of the dispersion curve $\omega = \omega(\beta)$ of the transmission band opened inside the band gap. Note that at

$\omega=\omega_B$ the dispersion curve has a flexing point, which means that second-order group velocity dispersion (i.e., $\partial^2\beta/\partial\omega^2$) vanishes at $\omega=\omega_B$ and pulse distortion is thus minimized at this frequency. The width $\Delta\omega_B$ of the transmission band can be generally written as

$$\Delta\omega_B = \frac{2\pi}{\Lambda_S}\frac{c_0}{n_0}F(\sigma), \tag{8}$$

where

$$\sigma = \Delta n\frac{\Lambda_S}{2\lambda_B} \tag{9}$$

is a dimensionless parameter that measures the grating strength, $\lambda_B=2\pi n_0/k_B$ is the central Bragg wavelength (in vacuum) at which the opened transmission band is centered, and $F(\sigma)$ is a monotonic decreasing function of σ, with $F(\sigma)\to 0$ as $\sigma\to\infty$, whose profile depends on the specific shape of $a(z)$ and can be calculated, in general, only numerically (see examples given below). The group velocity v_g of a pulse propagating in the grating at carrier frequency $\omega=\omega_B$ is given by

$$\frac{1}{v_g} = \left(\frac{\partial\beta}{\partial\omega}\right)_{\omega=\omega_B}. \tag{10}$$

Note that, as σ increases, the bandwidth $\Delta\omega_B$ of transmission window decreases and correspondingly the slope $\partial\omega/\partial\beta$ decreases, leading to light slowing down. An equivalent expression of the group velocity in terms of the envelopes u and v can be derived by the application of the Hellmann-Feynman theorem of quantum mechanics to the coupled-mode equations (3) and (4), as detailed in Appendix A (see also [19]):

$$\frac{1}{v_g} = \frac{n_0}{c_0}\frac{\int_0^{\Lambda_S} dz(|u|^2+|v|^2)}{\Lambda_S(|u|^2-|v|^2)}. \tag{11}$$

The expression of the group velocity as given by Eq. (11) can be useful in certain cases to analytically estimate the group velocity reduction factor, defined as

$$S = \frac{c_0/n_0}{v_g} = \frac{\int_0^{\Lambda_S} dz(|u|^2+|v|^2)}{\Lambda_S(|u|^2-|v|^2)}, \tag{12}$$

whenever the analytical expression of the fields u and v is available. An example is that of the Moiré grating, discussed below, for which an analytical expression of the band dispersion curve is not available. The group velocity reduction factor S turns out to be a function of the dimensionless grating strength σ solely.

The previous general considerations can be specialized by considering, as examples, three special superstructure profiles $a(z)$: the square-shaped profile, corresponding to a periodic sequence of π phase defects, the sinusoidal profile, corresponding to the Moiré superstructure [14], and the triangular-shaped profile (see Fig. 3). The behaviors of the normalized bandwidth $F(\sigma)$ [Eq. (8)] and group velocity reduction factor S versus the dimensionless parameter σ [Eq. (9)] for these superstructures are shown in Fig. 3; the plots have been obtained by a numerical computation of the dispersion curve $\beta=\beta(\omega)$ using Eq. (7), where the transmission field coefficient $t(\omega)$ of the single superstructure cell was numerically computed by a transfer matrix analysis of the coupled mode equations (3) and (4). Analytical expressions of the slowing down factor S can be given in the sinusoidal (Moiré grating) and in the square-shaped (phase defect grating) superstructure profiles. As shown in Appendix B, one has:

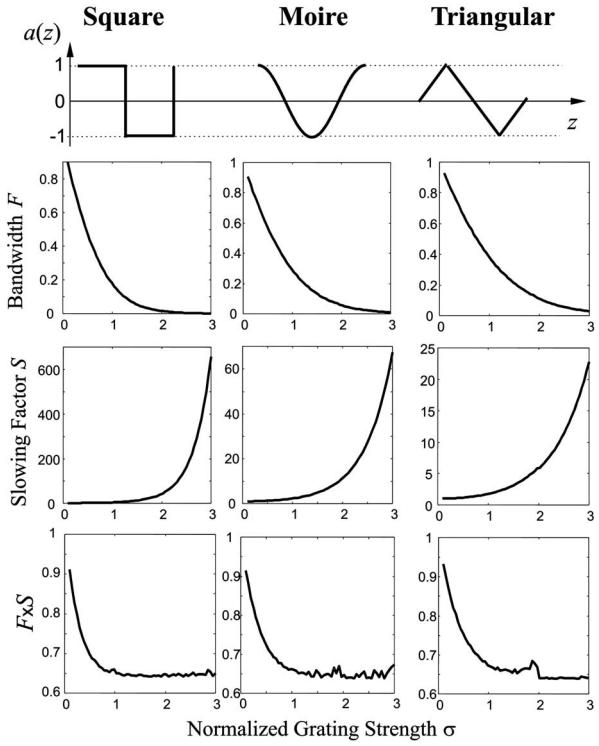

FIG. 3. Numerically computed behavior of normalized bandwidth F, group velocity reduction factor S, and $F\times S$ product versus the dimensionless parameter σ [see Eq. (9)] for three different superstructure profiles.

$$S = \frac{\sinh(\pi\sigma)}{\pi\sigma} \tag{13}$$

for the phase-defect grating, and

$$S = I_0(2\sigma), \tag{14}$$

for the Moiré grating, where I_0 is the modified Bessel function of zero order. Note that, as σ increases, the group velocity reduction factor S increases, however, the available bandwidth $\Delta\omega_B$ decreases, which is a general feature of slow-wave photonic structures (see, for instance, [3]). An important parameter is the ratio between the bandwidth $\Delta\omega_B$ and the group velocity v_g, which is proportional to the product $F\times S$. Such a quantity turns out to be not strongly dependent on σ (see Fig. 3), and may hence provide a quantitative estimate of the quality of the slow light superstructure. Note that the product $F\times S$ is almost the same for the three types

of superstructures, however for the square-shaped grating profile a given slowing down factor (and corresponding bandwidth) is achieved at lower values of grating strength σ. For the design of a slow-wave superstructure, it is interesting to observe that to get a desired group velocity reduction factor S, a given value of σ must be used. According to Eq. (9), for a maximum available refractive index change Δn, the superstructure period Λ_S is correspondingly determined, and hence the available bandwidth $\Delta\omega_B$ [see Eq. (8)]. Note that, since σ is proportional to Λ_S and the bandwidth $\Delta\omega_B$ is inversely proportional to Λ_S, to achieve large slowing down factors with a wide bandwidth, small values of Λ_S and high values of Δn are ultimately required.

Though the previous analysis has been concerned with an infinitely-long superstructure, similar results can be found by considering a finite superstructure composed by N cells. In this case, the determination of the spectral transmission curve and transmission group delay of the grating can be done by a direct numerical analysis of the coupled-mode equations (3) and (4) using standard techniques. To avoid the appearance of ripples in the group delay and power transmission spectral curves due to finite grating length effects (impedance mismatch), apodization profiles that envelope the periodic superstructure profile $a(z)$ are required as for uniform periodic gratings. Such a procedure is rather standard in designing grating with finite length and low ripples (see, for instance, [20,21], and references therein), and is hence not discussed in detail in this work.

III. EXPERIMENTAL RESULTS

In this section we provide an experimental demonstration of light slowing down in a superstructure Bragg grating, using a 20-cm-long Moiré fiber grating designed to operate at the 1.5 μm wavelength of optical communications. We first describe the design and fabrication of the Moiré fiber grating, and then present experimental measurements of group velocity pulse reduction with pulse durations down to the nanosecond scale.

A. Grating design and fabrication

The grating superstructure designed and fabricated to demonstrate group velocity reduction consists of a 20-cm-long Moiré grating UV written on a single-mode hydrogenated Ge–Si fiber using a periodic phase mask with a Bragg frequency at around $\lambda_B = 1533$ nm. The amplitude profile $a(z)$ of the designed superstructure is shown in Fig. 4(a). The designed superstructure period is $\Lambda_S = 2.5$ cm and the grating is composed by $N = 8$ cells. A raised cosine over 25% of total grating length at both grating ends is introduced as an apodization profile to smooth out group delay ripples. Figures 4(b) and 4(c) show the power transmission spectrum T (in dB units) and the group delay τ_g, respectively, of the designed grating, as numerically computed by a standard transfer matrix analysis of coupled-mode equations (3) and (4), assuming a maximum refractive index change $\Delta n \simeq 1.25 \times 10^{-4}$ and $n_0 = 1.464$. Note that the group delay τ_g far from resonance is $\tau_g \simeq 976$ ps, whereas at the center of the

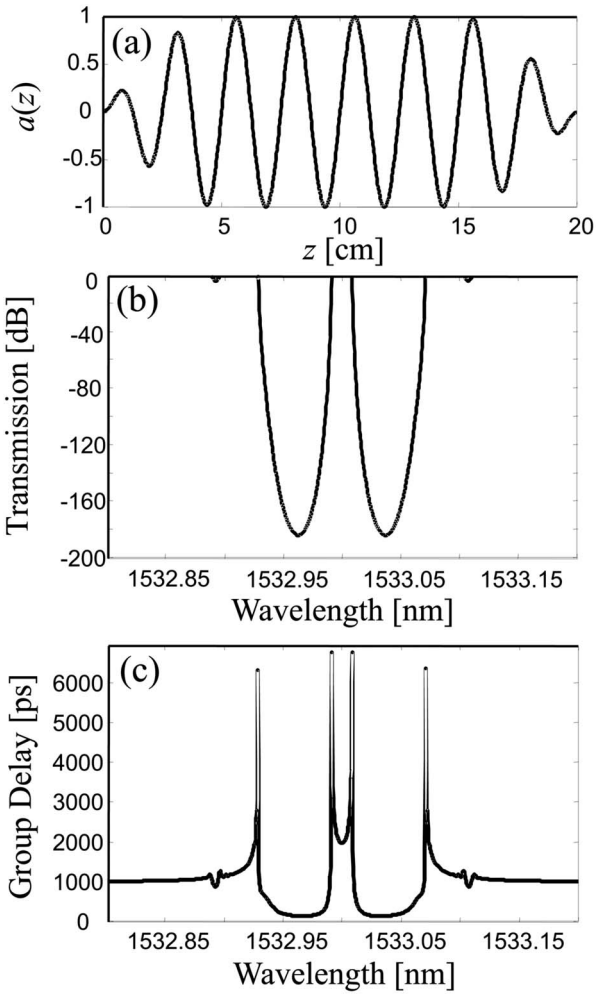

FIG. 4. (a) Amplitude profile of the 20-cm long Moiré grating designed for our experiment. (b) Numerically computed power spectral transmission of the grating (in logarithmic units). (c) Numerically-computed behavior of group delay (phase time) versus wavelength.

opened transmission band between the two band gaps the group delay is increased up to $\tau_g \simeq 1980$ ps, thus corresponding to an expected group velocity reduction factor $S \simeq 2.03$. Note that this slowing down factor is in quite good agreement with that predicted for an infinitely-long Moiré grating: for parameter values which apply to our structure, one has in fact $\sigma \simeq 1.02$ and correspondingly from Eq. (14) one obtains $S \simeq 2.34$. The slight lower value ($S \simeq 2.03$) for the slowing down factor obtained by the exact group delay curve of the finite grating [Fig. 4(c)] is mainly due to the apodization profile superimposed to the Moiré pattern, which is necessary to avoid the appearance of undesirable ripples causing pulse distortion.

The grating was fabricated using a continuous-writing technique [22,23] in which the UV beam from an intracavity frequency doubled Ar-ion laser, delivering about ~80 mW at 244 nm wavelength, is focused by a cylindrical lens onto the fiber core through a phase mask and is strobed using an acousto-optic modulator. With this writing technique, the fiber is continuously translated in front of the phase mask, and

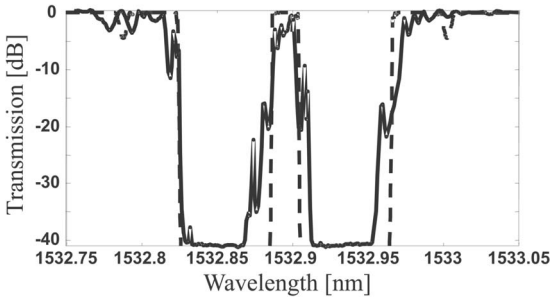

FIG. 5. Measured spectral power transmission of the fabricated Moiré grating (solid line). The dashed curve shows, for comparison, the transmission profile of the designed grating.

the fiber position is monitored by an interferometer, with submicrometer precision, which triggers the acousto-optic modulator with period corresponding to the desired grating pitch. This allows for an accurate exposure on a grating plane by grating plane basis. By suitably delaying adjacent exposures with respect to each other, the desired amplitude modulation profile $a(z)$ shown in Fig. 4(a) is achieved, with a spatial resolution of ~ 1 mm. A total fluence of ~ 0.3 kJ/cm^2 was used to write the grating. The spectral power transmission of the fabricated grating, shown in Fig. 5 (solid curve), was measured using a tunable semiconductor laser (Agilent Model 8164B) and a high precision wavemeter, with a wavelength resolution of 1 pm. The dashed curve in the figure corresponds to the power transmission predicted by the theory. Note that the lowest measured transmission level of $\simeq -40$ dB was due to the limited sensitivity of the power meter.

B. Pulse delay measurements

Direct time-domain measurements of group velocity reduction were performed in transmission experiments using probing optical pulses with a tunable temporal duration and wavelength. Pulse durations were chosen such that the spectral pulse bandwidth is less than or comparable with the transmission bandwidth (~ 1.5 GHz at -3 dB) of the Moiré grating. The experimental setup for delay time measurements is shown in Fig. 6. A pulse train, with variable repetition

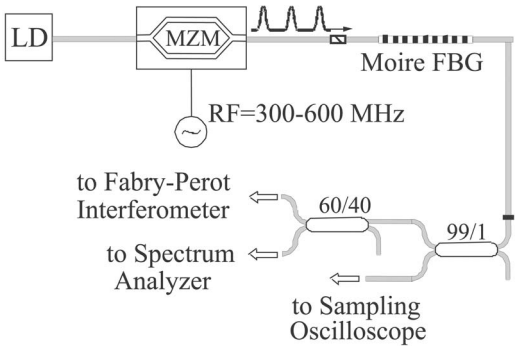

FIG. 6. Schematic of the experimental setup for pulse delay measurements. LD: tunable laser diode; MZM: Mach-Zehnder amplitude modulator; RF: radio frequency.

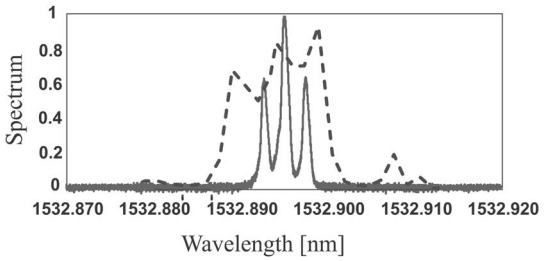

FIG. 7. Spectrum of the pulse train (solid curve, in arbitrary units), as measured by the Fabry-Perot interferometer, for $f_m = 300$ MHz. The dashed curve shows, for comparison, the transmission band (in linear units) of the Moiré grating.

frequency f_m and pulse duration, was generated by external modulation of a single-frequency continuous-wave tunable laser diode (Agilent Mod. 8164B), which allows for a fine wavelength tuning with a sensitivity of 0.1 pm, i.e., much smaller than the transmission bandwidth of the Moiré grating. The ~ 8 mW output power emitted by the laser diode was sent to a $LiNbO_3$-based Mach-Zehnder modulator, sinusoidally driven at a frequency f_m by a low-noise radio-frequency (RF) synthesizer. The bias point of the modulator and the RF modulation power level were chosen to generate a train of symmetric pulses without pedestals. By increasing the modulation frequency f_m from 300 to 600 MHz, a continuous tuning of pulse duration from $\simeq 1.2$ ns down to $\simeq 760$ ps can be achieved. The pulse train was simultaneously detected in the temporal domain, using a fast sampling oscilloscope (Agilent Mod. 86100A) with a low jitter noise and an impulsive response of $\simeq 15$ ps, and in the spectral domain, using an optical spectrum analyzer (Ando Model AQ6317C) with a resolution of 10 pm and a plane-plane Fabry-Perot interferometer (Burleigh Mod. RC-1101R) with a free-spectral range of ~ 5.4 GHz and a measured finesse of ~ 110. A portion of the sinusoidal RF signal that drives the Mach-Zehnder modulator was used as an external trigger for the oscilloscope, thus providing precise synchronism among successive pulses. The optical spectrum analyzer was used to coarsely tune the laser frequency at the transmission band of the Moiré grating, whereas the higher resolution provided by the Fabry-Perot interferometer allowed us to resolve the spectrum profile of the pulse train. A typical spectrum of the incident optical pulse, for a modulation frequency $f_m = 300$ MHz, is shown in Fig. 7; the corresponding pulse duration is $\simeq 1.2$ ns. Figure 8(a) shows typical temporal traces, averaged over 8 acquisitions, of the transmitted optical pulses when the laser frequency is tuned far from the Bragg wavelength of the grating (solid curve) and at the center of the transmission Moiré band (dashed curve) for $f_m = 300$ MHz. Note that, in the latter case, the pulse trace is delayed by $\simeq 1$ ns, with low pulse distortion, which is in good agreement with the temporal delay predicted for the designed grating. The corresponding group velocity reduction factor is $\simeq 2$. As the modulation frequency f_m is increased, and hence the pulse duration decreased, pulse distortion becomes more pronounced due to pulse spectral broadening, however, pulse delay is still visible for pulse durations below the nanosecond scale. As an example,

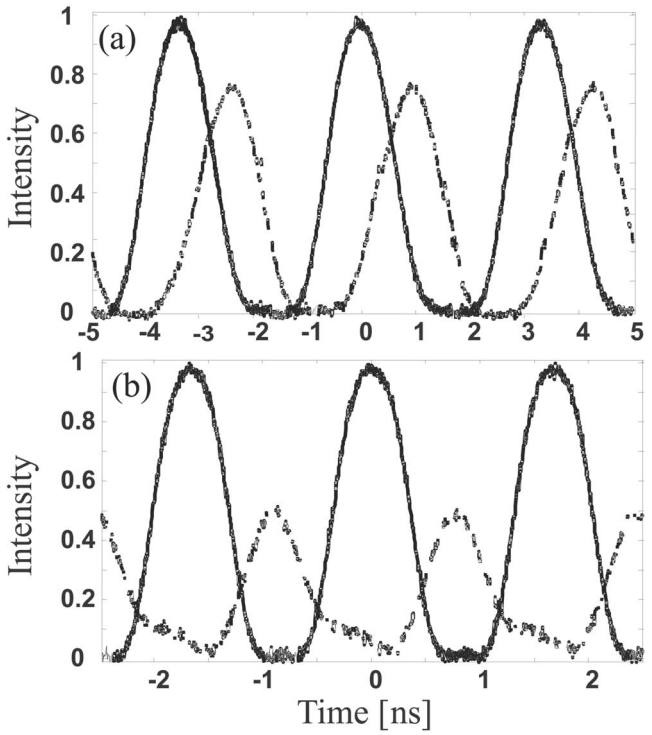

FIG. 8. Recorded oscilloscope traces of pulse trains when the laser frequency is tuned a few nanometers far from the Bragg frequency of the structure (solid curves) and at the center of the transmission band of the superstructure (dashed curves). In (a), modulation frequency is f_m=300 MHz (FWHM pulse duration ≃1.2 ns), in (b) f_m=600 MHz (FWHM pulse duration ≃0.76 ns).

Fig. 8(b) shows the recorded temporal traces, for an off-resonance pulse and for a pulse spectrally tuned inside the transmission band of the Moiré grating, corresponding to a modulation frequency f_m=600 MHz, i.e., to a pulse duration of ≃760 ps. Note that, despite considerable pulse distortion, the delayed pulse sequence is yet well distinguishable. We note that delays with low distortion of shorter pulses at higher repetition rates, which is of major interest for optical communication applications, could be obtained by designing and fabricating a Moiré grating with a shorter period Λ_S and a higher refractive index change Δn, which for our available fibers was limited to $\simeq 1.25\times 10^{-4}$. In principle, an increase of the refractive index change Δn by a factor of ~10 could be obtained using highly loaded hydrogenated fibers, allowing to achieve a slowing down factor $S\sim 2$ with a bandwidth ~15 GHz.

IV. CONCLUSIONS

In this work we have presented a theoretical analysis and an experimental demonstration of light slowing down in periodic superstructure Bragg gratings. Based on a coupled-mode equation analysis, a general analysis of slow-wave propagation in periodic superstructures has been reported, and specific results for square-shaped, sinusoidal, and triangular superstructures have been given. A 20-cm-long Moiré fiber grating has been fabricated by a continuous-writing technique, to show group velocity reduction at the 1.5 μm wavelength of optical communications. A slowing down factor of ≃2 has been demonstrated for optical pulses with subnanosecond temporal duration. Following the discussion of Sec. II, larger slowing down factors with shorter pulse durations may be achievable using optical fibers with a higher photosensitivity.

APPENDIX A

In this Appendix we derive the expression of the group velocity v_g in an infinitely-long grating, as given by Eq. (11) in the text, using a procedure which closely resembles the derivation of the Hellmann-Feynman theorem of quantum mechanics for a quantum system whose Hamiltonian depends on a parameter. To this aim, let us observe that the periodic part $|\mathbf{v}\rangle \equiv (\tilde{u},\tilde{v})^T$ of the Bloch-Floquet mode [Eq. (6)] for the coupled-mode equations (3) and (4) satisfies the following eigenvalue equation, which is readily obtained by substituting Eq. (6) into Eqs. (3) and (4):

$$\beta|\mathbf{v}\rangle = \mathcal{H}|\mathbf{v}\rangle, \tag{A1}$$

where the operator $\mathcal{H}$ is given by

$$\mathcal{H} = \begin{pmatrix} i\dfrac{d}{dz} + \delta & q(z) \\ -q(z) & i\dfrac{d}{dz} - \delta \end{pmatrix}. \tag{A2}$$

Note that, if we introduce the pseudoscalar product $\langle \mathbf{w}|\mathbf{v}\rangle \equiv (1/\Lambda_S)\int_0^{\Lambda_S} dz(w_1^* v_1 - w_2^* v_2)$, the operator $\mathcal{H}$ is self-adjoint, i.e., $\langle \mathbf{w}|\mathcal{H}\mathbf{v}\rangle = \langle \mathcal{H}\mathbf{w}|\mathbf{v}\rangle$. Note also that, since $\mathcal{H}$ depends parametrically on the wave number detuning δ, both eigenvalues β and eigenvectors $|\mathbf{v}\rangle$ of $\mathcal{H}$ depend on δ. If we take the scalar product of both sides of Eq. (A1) with $\langle \mathbf{v}|$, we obtain:

$$\beta = \frac{\langle \mathbf{v}|\mathcal{H}|\mathbf{v}\rangle}{\langle \mathbf{v}|\mathbf{v}\rangle}. \tag{A3}$$

Taking the derivative of both sides of Eq. (A3) with respect to δ, we get

$$\frac{\partial\beta}{\partial\delta} = \frac{1}{\langle \mathbf{v}|\mathbf{v}\rangle}\left(\frac{\partial\langle \mathbf{v}|\mathcal{H}|\mathbf{v}\rangle}{\partial\delta} - \beta\frac{\partial\langle \mathbf{v}|\mathbf{v}\rangle}{\partial\delta}\right). \tag{A4}$$

Since $\mathcal{H}$ is self-adjoint and taking into account that $\mathcal{H}|\mathbf{v}\rangle = \beta|\mathbf{v}\rangle$, one has:

$$\begin{aligned}\frac{\partial\langle \mathbf{v}|\mathcal{H}|\mathbf{v}\rangle}{\partial\delta} &= \left\langle \frac{\partial\mathbf{v}}{\partial\delta}|\mathcal{H}|\mathbf{v}\right\rangle + \left\langle \mathbf{v}|\mathcal{H}|\frac{\partial\mathbf{v}}{\partial\delta}\right\rangle + \left\langle \mathbf{v}\left|\frac{\partial\mathcal{H}}{\partial\delta}\right|\mathbf{v}\right\rangle \\ &= \left\langle \mathbf{v}\left|\frac{\partial\mathcal{H}}{\partial\delta}\right|\mathbf{v}\right\rangle + \beta\frac{\partial\langle \mathbf{v}|\mathbf{v}\rangle}{\partial\delta}\end{aligned} \tag{A5}$$

and hence, substitution of Eq. (A5) into Eq. (A4) yields

$$\frac{\partial\beta}{\partial\delta} = \frac{\left\langle \mathbf{v}\left|\dfrac{\partial\mathcal{H}}{\partial\delta}\right|\mathbf{v}\right\rangle}{\langle \mathbf{v}|\mathbf{v}\rangle}. \tag{A6}$$

From Eq. (A2) we have

$$\frac{\partial \mathcal{H}}{\partial \delta} = \begin{pmatrix} 1 & 0 \\ 0 & -1 \end{pmatrix}, \tag{A7}$$

so that Eq. (A6) reads explicitly

$$\frac{\partial \beta}{\partial \delta} = \frac{\int_0^{\Lambda_S} dz(|\tilde{u}|^2 + |\tilde{v}|^2)}{\int_0^{\Lambda_S} dz(|\tilde{u}|^2 - |\tilde{v}|^2)}. \tag{A8}$$

Taking into account that $|\tilde{u}|=|u|$, $|\tilde{v}|=|v|$, and that $|u|^2-|v|^2$ is constant, using the relation $1/v_g=\partial\beta/\partial\omega=(\partial\beta/\partial\delta)(\partial\delta/\partial\omega)=(n_0/c_0)(\partial\beta/\partial\delta)$, one finally obtains Eq. (11) given in the text.

APPENDIX B

In this Appendix we derive the analytical expressions for the group velocity reduction factor $S=(c_0/n_0)/v_g$ in the case of a square-shaped (phase-defect grating) and sinusoidal (Moiré grating) superstructures.

1. The phase-defect superstructure

In this case the transfer matrix of the single superstructure cell can be calculated analytically as the product of the transfer matrices of two uniform gratings with a π phase shift between them, namely

$$\begin{pmatrix} \frac{1}{t^*} & -\frac{r^*}{t^*} \\ -\frac{r}{t} & \frac{1}{t} \end{pmatrix} = \begin{pmatrix} \cosh(\pi\xi) + i\frac{\delta'}{\xi}\sinh(\pi\xi) & i\frac{\sigma}{\xi}\sinh(\pi\xi) \\ -i\frac{\sigma}{\xi}\sinh(\pi\xi) & \cosh(\pi\xi) - i\frac{\delta'}{\xi}\sinh(\pi\xi) \end{pmatrix} \times \begin{pmatrix} \cosh(\pi\xi) + i\frac{\delta'}{\xi}\sinh(\pi\xi) & -i\frac{\sigma}{\xi}\sinh(\pi\xi) \\ i\frac{\sigma}{\xi}\sinh(\pi\xi) & \cosh(\pi\xi) - i\frac{\delta'}{\xi}\sinh(\pi\xi) \end{pmatrix}, \tag{B1}$$

where we have set $\delta'=\delta\Lambda_S/(2\pi)$ and $\xi=(\sigma^2-\delta'^2)^{1/2}$. From Eq. (B1) one readily obtains

$$\frac{1}{t^*} = 1 - 2\frac{\delta'^2}{\xi^2}\sinh^2(\pi\xi) - 2i\frac{\delta'}{\xi}\cosh(\pi\xi)\sinh(\pi\xi). \tag{B2}$$

The dispersion relation $\beta=\beta(\omega)$, given by Eq. (7), then reads explicitly

$$\cos(\beta\Lambda_S) = 1 - 2\frac{\delta'^2}{\xi^2}\sinh^2(\pi\xi). \tag{B3}$$

In order to calculate $(\partial\beta/\partial\omega)$ at $\omega=\omega_B$, let us approximate the behavior of $\beta(\omega)$ in the neighborhood of $\omega=\omega_B$, i.e., of $\delta'=0$, and hence of $\beta=0$; the leading order expansion of Eq. (B3) then yields $\beta\simeq 2\delta'\sinh(\pi\sigma)/(\sigma\Lambda_S)$, i.e.,

$$\beta \simeq \frac{n_0}{c_0}(\omega-\omega_B)\frac{\sinh(\pi\sigma)}{\pi\sigma}. \tag{B4}$$

Using Eq. (B4), for the group velocity at $\omega=\omega_B$ we then finally get

$$\frac{1}{v_g} = \left(\frac{\partial\beta}{\partial\omega}\right)_{\omega=\omega_B} = \frac{n_0}{c_0}\frac{\sinh(\pi\sigma)}{\pi\sigma}, \tag{B5}$$

which gives for the group velocity reduction factor S the expression (13) given in the text.

2. The Moiré superstructure

In this case, since an analytical expression of the transfer matrix (and hence of the spectral field transmission t) is not available, it is more convenient to calculate the group velocity reduction factor S using Eq. (12) given in text, which requires the knowledge of the field profiles u and v along the grating. We note that, for $\omega=\omega_B$, i.e., for $\delta=0$, the coupled-mode equations (3) and (4) with $a(z)=\cos(2\pi z/\Lambda_S)$ admit of the following solution, satisfying the boundary conditions $u(0)=1$ and $v(0)=0$,

$$u(z) = \tilde{u}(z) = \cosh[\sigma\sin(2\pi z/\Lambda_S)], \tag{B6}$$

$$v(z) = \tilde{v}(z) = -i\sinh[\sigma\sin(2\pi z/\Lambda_S)].$$

Taking into account the identity

$$\frac{1}{2\pi}\int_0^{2\pi} dz\exp(\pm 2\sigma\sin z) = I_0(2\sigma), \tag{B7}$$

where I_0 is the modified Bessel function of zero order, the substitution of Eq. (B6) into Eq. (12) yields, after some algebra, Eq. (14) given in the text.

[1] R. W. Boyd and D. J. Gauthier, *Progress in Optics 43*, edited by E. Wolf (Elsevier, Amsterdam, 2002), Chap. 6, p. 497.
[2] *Nontraditional Forms of Light*, edited by A. Dogariu, P. W. Milonni, L. Wang, and H. G. Winful, special issue of IEEE J. Sel. Top. Quantum Electron. 9, 1 (2003).
[3] J. B. Khurgin, J. Opt. Soc. Am. B **22**, 1062 (2005).
[4] J. Scheuer, G. T. Paloczi, J. K. S. Poon, and A. Yariv, Opt. Photonics News **16**, 36 (2005).
[5] S. Longhi, M. Marano, M. Belmonte, and P. Laporta, IEEE J. Sel. Top. Quantum Electron. **9**, 4 (2003).
[6] N. Brunner, V. Scarani, M. Wegmüller, M. Legre, and N. Gisin, Phys. Rev. Lett. **93**, 203902 (2004).
[7] K. Y. Song, M. G. Herraez, and L. Thevenaz, Opt. Express **13**, 82 (2004).
[8] Y. Okawachi, M. S. Bigelow, J. E. Sharping, Z. Zhu, A. Schweinsberg, D. J. Gauthier, R. W. Boyd, and A. L. Gaeta, Phys. Rev. Lett. **94**, 153902 (2005).
[9] A. Melloni, F. Morichetti, and M. Martinelli, Opt. Quantum Electron. **35**, 365 (2003).
[10] J. K. S. Poon, J. Scheuer, Y. Xu, and A. Yariv, J. Opt. Soc. Am. B **21**, 1665 (2004).
[11] H. Altug and J. Vuckovic, Appl. Phys. Lett. **86**, 111102 (2005).
[12] H. Gersen, T. J. Karle, R. J. P. Engelen, W. Bogaerts, J. P. Korterik, N. F. van Hulst, T. F. Krauss, and L. Kuipers, Phys. Rev. Lett. **94**, 073903 (2005).
[13] S. Longhi, M. Marano, P. Laporta, O. Svelto, and M. Belmonte, J. Opt. Soc. Am. B **19**, 2742 (2002).
[14] J. B. Khurgin, Phys. Rev. A **62**, 013821 (2000).
[15] R. Shimada, T. Koda, T. Ueta, and K. Ohtaka, J. Appl. Phys. **90**, 3905 (2001).
[16] We note that previous theoretical works on light slowing down and localization in superstructure Bragg gratings [14,15] have not used a coupled-mode equation analysis and have been limited mostly to a dual-period (i.e. Moiré) grating structure. We also note that, though coupled-mode equations are usually derived for a shallow grating, they may be accurate even for deep gratings (see, for instance, [17]).
[17] J. E. Sipe, L. Poladian, and C. M. de Sterke, J. Opt. Soc. Am. A **11**, 1307 (1994).
[18] J. M. Bendickson, J. P. Dowling, and M. Scalora, Phys. Rev. E **53**, 4107 (1996).
[19] K. Sakoda, *Optical Properties of Photonic Crystals* (Springer-Verlag, Berlin, 2001), Sec. 2.6, p. 32. It should be noted that the expression of the group velocity, as given by Eq. (11), is consistent with the result that in a periodic structure the group velocity is equal to the energy velocity of light, which is defined as the ratio between the spatial averages of the Poyinting vector and of the energy density of the electromagnetic field [see P. Yeh, J. Opt. Soc. Am. **69**, 742 (1979)]. Light slowing down thus corresponds to strong localization of the electromagnetic energy density in the medium.
[20] K. Ennser, N. Zervas, and R. L. Laming, IEEE J. Quantum Electron. **34**, 770 (1998).
[21] M. Ibsen, M. K. Durkin, and R. I. LAming, IEEE Photonics Technol. Lett. **10**, 84 (1998).
[22] W. H. Loh, M. J. Cole, M. N. Zervas, S. Barcelos, and R. I. Laming, Opt. Lett. **20**, 2051 (1995).
[23] A. Asseh, H. Storoy, B. E. Sahlgren, S. Sandgan, and R. A. H. Stubbe, J. Lightwave Technol. **15**, 1419 (1997).